Environ Sci Pollut Res
DOI 10.1007/s11356-016-6727-9

RESEARCH ARTICLE

Dust aerosol properties and radiative forcing observed in spring during 2001–2014 over urban Beijing, China

Xingna Yu[1] · Rui Lü[1] · K. Raghavendra Kumar[1] · Jia Ma[1,3] · Qiuju Zhang[2] · Yilun Jiang[3] · Na Kang[1] · Suying Yang[1] · Jing Wang[1] · Mei Li[4]

Received: 19 November 2015 / Accepted: 19 April 2016

Abstract The ground-based characteristics (optical and radiative properties) of dust aerosols measured during the springtime between 2001 and 2014 were investigated over urban Beijing, China. The seasonal averaged aerosol optical depth (AOD) during spring of 2001–2014 was about 0.78 at 440 nm. During dust days, higher AOD occurred associated with lower Ångström exponent (AE). The mean $AE_{440–870}$ in the springtime was about 1.0, indicating dominance of fine particles over the region. The back-trajectory analysis revealed that the dust was transported from the deserts of Inner Mongolia and Mongolia arid regions to Beijing. The aerosol volume size distribution showed a bimodal distribution pattern, with its highest peak observed in coarse mode for all episodes (especially for dust days with increased volume concentration). The single scattering albedo (SSA) increased with wavelength on dust days, indicating the presence of more scattering particles. Furthermore, the complex parts (real and imaginary) of refractive index showed distinct characteristics with lower imaginary values (also scattering) on dust days. The shortwave (SW; 0.2–4.0 μm) and longwave (LW; 4–100 μm) aerosol radiative forcing (ARF) values were computed from the Santa Barbara DISORT Atmospheric Radiative Transfer (SBDART) model both at the top of atmosphere (TOA) and the bottom of atmosphere (BOA) during dust and non-dust (dust free) days, and the corresponding heating rates and forcing efficiencies were also estimated. The SW (LW) ARF, therefore, produced significant cooling (warming) effects at both the TOA and the BOA over Beijing.

Keywords Beijing · Dust aerosols · AOD · Single-scattering albedo · Aerosol radiative forcing · Forcing efficiency

Responsible editor: Gerhard Lammel

Electronic supplementary material The online version of this article (doi:10.1007/s11356-016-6727-9) contains supplementary material, which is available to authorized users.

✉ K. Raghavendra Kumar
kanike.kumar@gmail.com; krkumar@nuist.edu.cn

✉ Mei Li
limei2007@163.com

[1] Key Laboratory of Meteorological Disaster, Ministry of Education (KLME)/Joint International Research Laboratory of Climate and Environment Change (ILCEC)/Collaborative Innovation Center on Forecast and Evaluation of Meteorological Disasters (CIC-FEMD)/ Key Laboratory for Aerosol-Cloud-Precipitation of China Meteorological Administration, Nanjing University of Information Science and Technology, Nanjing 210044, China

[2] Baoshan District Center for Disease Control and Prevention, Shanghai 201901, China

[3] Guangzhou Hexin Analytical Instrument Company Limited, Guangzhou 510530, China

[4] Institute of Atmospheric Environment Safety and Pollution Control, Jinan University, Guangzhou 510632, China

Introduction

There is great difficulty in characterizing the aerosol optical and microphysical properties resulting in a large uncertainty in the radiative forcing of climate (Valenzuela et al. 2015). The impact of atmospheric aerosols on radiative forcing is still remaining highly uncertain due to their great spatial and temporal variability and the large variability in composition, size distribution, particle shape, and vertical distribution (IPCC 2013). Dust aerosol is one of the greatest uncertainties on radiative forcing; it may either absorb or scatter radiation resulting in either “positive forcing” or “negative forcing” and influencing the radiation budget (Alpert et al. 1998; Liao and Seinfeld 1998; Miller et al. 2004). Mineral dust

Published online: 27 April 2016

aerosols reflect shortwave (SW) radiation within the atmospheric window channel back into space resulting in cooling of the Earth's system, but longwave (LW) radiation is absorbed resulting in a warming effect (Prasad and Singh 2007; Alam et al. 2012; Cao et al. 2014). Meanwhile, dust aerosol can influence the air quality, meteorological and atmospheric parameters, hydrologic cycle, and monsoon system (Ramanathan et al. 2001; Tegen et al. 2004; Lau et al. 2006; Alam et al. 2014b; Cao et al. 2014). Also, they can reduce atmospheric visibility and correspondingly enhance health risks (Zhuang et al. 2001).

Beijing, the capital of China, is one of the most populous cities in the world with a population of 21 million (as of the population census records in 2013) covering an area of 16, 800 km^2. It is located at the foothills of Yan Mountains and Taihang Mountains, in the North China Plain. The climate of Beijing is known as "continental monsoon" and has four distinct seasons each year as demonstrated by Xia et al. (2006). Dust storms occur annually during the spring season (March, April, May (MAM)), and large quantities of aeolian dust are transported to downwind regions of north China (Cao et al. 2014). Beijing occasionally is impacted by these dust episodes transported by northwesterly and westerly winds from the Kumutage and the Taklimakan Deserts in western China or by northerly winds from the Mongolian Deserts (Cao et al. 2014). For example, the severe pollution events induced by dust reached 53 episodes in Beijing during 2000–2010 (Li et al. 2012). Xu et al. (2012) reported that there were 15 dusty days occurred in Beijing during spring of 2010, with increased air pollution index (API) up to 500 μg m^{-3} and hourly concentrations of particulate matter with aerodynamic diameter of ≤10 μm (PM_{10}) exceeded to 1500 μg m^{-3}. During dust event of 16–20 April 2006 over Beijing, a pronounced increase in hourly PM_{10} concentrations was observed which are up to 1200 μg m^{-3} (Wang et al. 2010). Another dust event of 26 April–3 May 2012, the API increased up to 473 μg m^{-3} (Shen et al. 2013). Recently, Cao et al. (2014) also reported the transport and characteristics of dust storms and changes in atmospheric parameters along their transport during 2005–2010 over Beijing.

Many researchers in the past studied aerosol optical properties including different aerosol types (such as haze, dust, biomass burning, and ocean/sea salt) in the global using ground- and satellite-based observations (Cao et al. 2014; Dubovik et al. 2002; Smirnov et al. 2002; Singh et al. 2004; Xia et al. 2006; Lee et al. 2010; Yu et al. 2011, 2012, 2013; Alam et al. 2011, 2014a, b; Valenzuela et al. 2012, 2015; Yan et al. 2015). These efforts have led to a good understanding of the impacts of dust aerosol on air quality, the hydrologic cycle, and the global climate effect. However, the previous studies in time span were mainly short-term characteristics of aerosols; the long-term (over 10 years) characteristics in aerosol optical properties were rather limited. In the present work, we have studied the characteristics of aerosol optical, microphysical, and radiative properties during dust and non-dust (dust free) episodes in atmospheric column using ground-based observations during major dust storm events (2001–2014) (see Table 1) over urban Beijing, China. The pathways and possible source regions for the dust storm events were also investigated by back-trajectory analysis using a Hybrid Single-Particle Lagrangian Integrated Trajectory (HYSPLIT) model. In addition to the aerosol characteristics, the aerosol radiative forcing (ARF) values at the earth's surface/bottom of atmosphere (BOA) and the top of atmosphere (TOA) and the aerosol radiative forcing efficiency (ARFE) were calculated during different dust intrusion episodes and non-dust (dust free) conditions using the Santa Barbara DISORT Atmospheric Radiative Transfer (SBDART) model (Ricchiazzi et al. 1998).

Instrumentation and measurements

Surface observations

The API simplifies the concentrations of several air pollutants to characterize air pollution level and air quality status in several levels (Zheng et al. 2014). It is related to the health impacts (Cao et al. 2014). For more information on API levels, the readers are requested to refer Table 1 of Cao et al. (2014) and hence not repeated here. The API data for the period 2001–2012 over Beijing is taken from the website of China National Environmental Monitoring Centre (CNEMC) (http://www.cnemc.cn/citystatus/airMap.jsp). All the local time (LT), hereafter, employed in this study is 8 h ahead of UTC.

Table 1 The dust days selected in springtime of Beijing during 2001–2014

Year	March	April	May
2001	24	–	1, 2, 3, 4, 5, 14
2002	–	–	–
2003	–	14	–
2004	14, 15, 27, 28	–	–
2005	–	29, 30	–
2006	10, 30, 31	9, 10, 11, 16, 22, 23, 24	16, 17
2007	–	30	–
2008	–	–	28
2009	13, 15, 16	–	–
2010	–	3, 4, 8	2, 7, 8, 9
2011	–	30	–
2012	29	27, 28, 29	–
2013	–	7, 8	–
2014	17	–	27

AErosol RObotic NETwork

The AErosol RObotic NETwork (AERONET) is a network of ground-based sun photometers to measure aerosol optical properties and validate satellite retrievals of aerosol optical properties (Holben et al. 1998; Alam et al. 2014a; Yu et al. 2016 and references here in). The CIMEL CE-318 automatic sun/sky radiometer, which is part of AERONET, was installed on the roof of the Institute of Atmospheric Physics (IAP) building in Beijing (39.98° N, 116.38° E; 92 m above sea level). The sun and sky radiometer is used for measuring direct sun and diffuse sky radiances within the 340–1020- and 440–1020-nm spectral ranges, respectively, with a 1.2° full field of view (Holben et al. 1998). The CE-318 performs automatic direct sun extinction measurements at about 15-min intervals regardless of cloud or clear sky during daytime given successful tracking of the Sun. Each Sun observation is composed of triplet measurements made over a 1-min interval for the above spectral bands which can be used to identify presence of clouds, if the triplet variation is beyond a certain threshold (adapted from Smirnov et al. 2000). The sun measurements were used to accurately calculate the aerosol optical depth (AOD), Ångström exponent (AE), and water vapor (WV), while spectrally dependent single scattering albedo (SSA), asymmetry factor (ASY), and complex index of refraction were obtained from both sky radiance almucantar measurements and direct sun measurements. An inversion algorithm was used to retrieve aerosol volume size distribution for the column of atmosphere within 22 bins for particle radius from 0.05 to 15 μm. The detailed aerosol properties retrieved were used for calculating broad band fluxes within the spectral range from 0.2 to 4.0 μm.

For the present study, we have used AERONET level 2.0 data (http://aeronet.gsfc.nasa.gov/) from both direct sun and inversion products for major dust episodes in spring during 2001–2014. The uncertainty in AOD retrieval under cloud free conditions was <±0.01 for wavelengths >440 nm and <±0.02 for shorter wavelengths, which is less than the ±5 % uncertainty for the retrieval of sky radiance measurements (Dubovik et al. 2000). Retrieval errors in volume size distribution typically do not exceed 15–35 % (depending on the aerosol type) for each particle radius bin within the 0.1–7.0-μm range. The errors for very small particle (0.05–0.1 μm) and very larger particles (7–15 μm) may be as large as 35–100 % for a given particle radius bin. SSAs were expected to have an uncertainty of 0.03–0.05 depending on aerosol type and loading (Dubovik et al. 2000; Alam et al. 2011, 2012; Yu et al. 2016). To avoid large inversion errors from the limited information content, these estimated errors with high aerosol loading (AOD_{440} ≥0.4) at a solar zenith angle greater than 50° were retained in this study. The retrieval accuracy and uncertainties have been explained in detail by Dubovik et al. (2002) and hence not repeated. We have also used the moderate resolution imaging spectroradiometer (MODIS), the Cloud-Aerosol Lidar and Infrared Pathfinder Satellite Observation (CALIPSO) (www.calispo.larc.nasa.gov; Winker et al. 2003), and the Hybrid Single-Particle Lagrangian Integrated Trajectory (HYSPLIT) model (http://ready.arl.noaa.gov/HYSPLIT.php; Draxler and Rolph 2013) to support the severe dust events measured using ground observations during the study period (see Supplementary Material (SM)).

Estimation of aerosol radiative forcing, efficiency, and heating rate

The aerosol radiative forcing (ARF) at the TOA or the BOA is defined as the difference in the net (down minus up) solar flux (in W m^{-2}) with and without aerosol, i.e.,

$$\Delta F = \left(F_{a\downarrow} - F_{a\uparrow}\right) - \left(F_{0\downarrow} - F_{0\uparrow}\right) \quad (1)$$

where ΔF denotes the ARF (in W m^{-2}) and F_a and F_0 denote the global irradiances with aerosol and without aerosols, respectively, either at the TOA or at the BOA. Further, the resultant net atmospheric forcing (ΔF), which also represents the amount of solar energy absorbed by aerosols in the atmosphere, was obtained by the difference between TOA and BOA. In this study, we have computed the net flux at the TOA and BOA separately both with and without aerosols, within the wavelength range for shortwave (SW; 0.2–4.0 μm) and longwave (LW; 4–100 μm) wavelengths, using the SBDART model (Ricchiazzi et al. 1998).

The SBDART model was developed by the atmospheric science community and has been widely used for radiative transfer calculations by several authors (e.g., Adesina et al. 2014; Alam et al. 2011, 2012, 2014a, b; Srivastava et al. 2015; Yu et al. 2016). Based on the prevailing weather conditions and measured parameters, we set the input in the atmospheric model as "mid-latitude summer." The crucial input parameters for the estimations of ARF were AOD, AE, SSA, ASY, and surface albedo, taken from the sun-sky radiometer of AERONET Beijing site (except the albedo). Other input parameters in the model include solar zenith angle, which is calculated using a small code in the SBDART model by specifying a particular date, time, latitude, and longitude. The column ozone concentration and surface albedo values were obtained from the Ozone Monitoring Instrument (OMI) onboard NASA's Aura satellite through the Giovanni online data system, developed and maintained by the NASA GES DISC (http://giovanni.nasa.gov/).

The atmospheric heating rate due to aerosol absorption into the atmosphere (i.e., ΔF) is calculated from the first law of thermodynamics and hydrostatic equilibrium (Liou 2002) as

$$\frac{\partial T}{\partial t} = \frac{g}{C_p} \times \frac{\Delta F}{\Delta P} \times 24(\mathrm{h/day}) \times 3600(\mathrm{s/h}) \quad (2)$$

where $\frac{\partial T}{\partial t}$ is the atmospheric heating rate (HR) in Kelvin per day (K day^{-1}), $\frac{g}{C_p}$ is the lapse rate where g is the acceleration due to gravity and C_p is the specific heat capacity of air at constant pressure (i.e., 1006 Jkg^{-1} K^{-1}) and ΔP is the atmospheric pressure difference between top and bottom boundaries of the atmosphere (Srivastava et al. 2015; Yu et al. 2016).

Results and discussion

Variations of aerosol optical depth and Ångström exponent

The AOD is representative of the airborne aerosol loading in the atmospheric column, and the AE indicates the size of particle, with a smaller AE represents abundance of coarse aerosol particles and vice versa. Figure 1 presents the averaged value of AOD at 440 and 1020 nm together with the $AE_{440–870\ nm}$ during the springtime of Beijing from 2001 to 2014. The averaged AOD_{440} (AOD_{1020}) in springtime during dust storm (2001–2014) events was generally higher (>0.4) and varied from 0.45 to 1.12 (from 0.20 to 0.65). In the present study, the seasonal averaged AOD_{440} (AOD_{1020}) during springtime of 2001–2014 was about 0.78 (0.42) over urban Beijing. The maximum seasonal mean AOD_{440} reached 1.12 in 2007, which is close to the annual averaged value of 1.06 for the year of 2007 (Yu et al. 2009). The values were larger than the measurements observed over an urban–industrial city, Kanpur in summer (Singh et al. 2004), a suburban agricultural site of Shengyang City during 2004–2007 (Wang et al. 2011), and the Tibetan Plateau in spring using ~10 years of multi-angle imaging spectroradiometer (MISR) aerosol data (Xu et al. 2015). Also, Alam et al. (2014b) investigated that the AOD_{440} values were greater than 2.0 during severe dust episodes in March 2012 at Lahore. The seasonal averaged value of $AE_{440–870}$ has not showed a distinct change from the long-term variation trend and was mostly greater than 1.0 (except in 2001 and 2006) (see Fig. 1), indicating that the fine particles were dominated during the spring over Beijing.

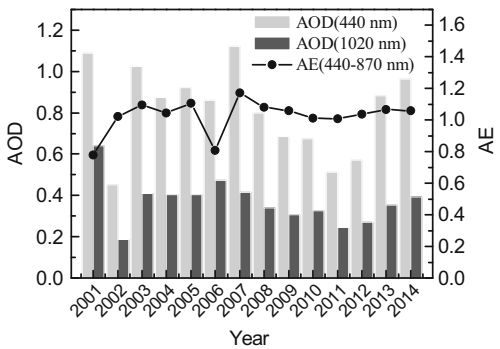

Fig. 1 The average AOD (at 440 and 1020 nm) and $AE_{440–870}$ during the spring season over Beijing from 2001 to 2014

Figure 2a shows the average AOD at four wavelengths between 440and 1020 nm, $AE_{440–870}$, and WV for different episodes over Beijing from 2001 to 2014. The AOD showed a decreasing trend with increasing wavelengths for all episodes (Fig. 2a). The averaged AOD_{440} during dust events/days that occurred in Beijing was up to 1.20, which is about 37 % larger than that of non-dust days and entire spring season. However, the $AE_{440–870}$ showed an opposite trend compared to that of AOD_{440}. A contrast in AE values during dust and non-dust days is clearly seen. For example, the minimum value of $AE_{440–870}$ occurred on dust days, with an average value of 0.44, which is about 2.4 times lower than the average $AE_{440–870}$ observed on non-dust days and the springtime. These results can be attributed to the major contribution of coarse aerosol particles on dust days and the dominance of fine particles during non-dust days. The mean value of $AE_{440–870}$ observed in springtime during 2001–2014 was about 1.0, which is lower than 4-year measurements conducted at Tongyu (Wu et al. 2015). The results were in good agreement with the observations reported by Eck et al. (2005)

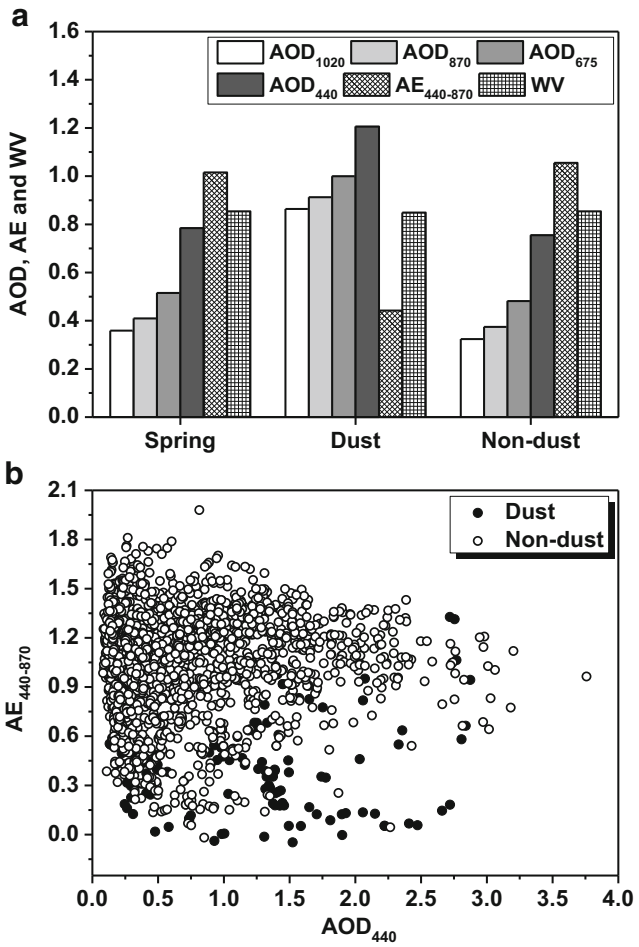

Fig. 2 Variations of aerosol optical properties for different episodes: **a** AOD at different wavelengths, AE, and WV (in cm) and **b** scatter plot of AOD vs. AE

representing minimum AE during springtime associated with dust storm activities. WV was almost consistent for the different episodes.

The scatter plot of AOD_{440} and $AE_{440–870}$ during dust and non-dust days is shown in Fig. 2b. The AE values were below 0.6 with AOD range of 0.25–2.80, and ~20 % of AE values were larger than 0.6, with high AOD during dust events, indicating the co-existence of coarse dust particles and fine pollution particles over the dust downwind region, despite that dust storms strike over the Beijing City. The lowest AE was observed on 23 April 2006, which is less than zero (negative). Negative values of AE indicate the more abundance of coarse desert dust particles during the dust outbreak episode. Similar AE values were also reported by Xia et al. (2004), Cao et al. (2014), and Singh et al. (2004) during severe dust events that occurred over Dunhuang, Beijing, and Kanpur. Eck et al. (2005) also found similar results in East Asia, with minimum AE during springtime associated with dust storm activities. Alam et al. (2012) examined the relationship between absorption AE (AAE) and extinction AE (EAE) and found the dominance of mineral dust aerosols over urban environments in Pakistan. A contrast in AE values during dust and non-dust days is clearly seen (see Fig. 2a). During non-dust days, the AE values were almost above 0.6 and the AOD mainly concentrated in a range from 0.25 to 1.50.

Figure 3a presents the average AOD, AE, and API values during major dust days in Beijing. As shown in Fig. 3a, the mean AOD showed extreme high values exceeding 1.4 on extreme dust days, with the mass concentration of PM_{10} greater than 450 μg m^{-3}. The API values were also found to be high (> 200) representing poor air quality, which is similar with the results reported by Cao et al. (2014) over Beijing during 2005–2010. Notably, high values of AOD and API were clearly depicted on April 10, 2006, up to 2.33 and 500, respectively, illustrating a high aerosol loading in the atmospheric column and serious impact on public health.

Figure 3b demonstrates the dominance of fine mode ($0.05 < r < 0.6$ μm) and coarse mode ($0.6 < r < 15$ μm) of AOD at 500 nm for the major dust days. It can be inferred from the figure that the coarse mode AOD during dust days increased dramatically. The coarse mode AOD exceeded 1.0 for all dust days and reached 1.83 on 4 May 2001, which is nearly 4.5 times higher than that of fine-mode AOD, indicating the dominant contribution of coarse particles due to dust outbreak events. This results in the low value of corresponding AE on all dust days. For example, the daily values of AE were usually lower than 0.4 and the lowest daily mean of 0.13 was depicted on 24 March 2001, 4 May 2001, and 28 March 2004. In contrast with other dust days, AE showed a high value (> 1.0) on 10 April 2006, suggesting increased fraction of fine particles and fine-mode AOD. This is characteristic of bimodal size distributions as suggested by Eck et al. (2005). It is also observed that the extinction percent of coarse particles

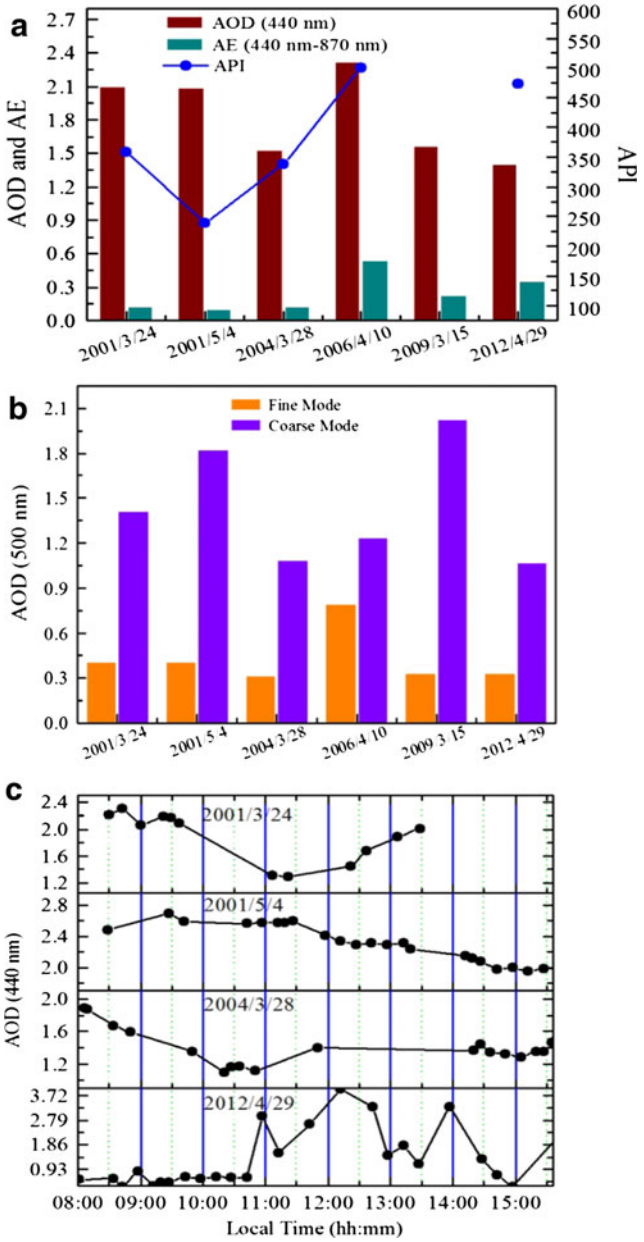

Fig. 3 Variations of aerosol optical properties over Beijing during severe dust days. **a** AOD, AE, and API; **b** daily AERONET AOD at 500 nm for fine and coarse modes; and **c** diurnal variations of AOD_{440}

out of total particles were greater than 40 % during dust days in springtime of Beijing, indicating that the coarse particle extinction has a greater contribution to the total extinction (see Fig. S1 of SM).

The diurnal AOD_{440} variability on major dust days is shown in Fig. 3c. The AOD_{440} values were generally larger than 1.0 (small AE) when the severe dust storm events struck the Beijing City. The figure reveals that the instantaneous maximum AOD over Beijing was up to ~4.0 that occurred on 29 April 2012. The severe dust was observed on 15 March 2009 over the north China and extended toward the eastern China, with the dust plumes (tan color suggests

primarily of dust) captured by the MODIS Terra satellite. The HYSPLIT back-trajectory analysis revealed that the air masses reached Beijing from the northwest areas such as the western area of Inner Mongolia, Xinjiang, and Gansu regions. Further, the CALIPSO retrieval on 15 March 2009 also confirmed that a well-mixed dust aerosol layer that occurred over the Beijing region in North China includes aerosol types of both dust and polluted dust (see Fig. S2 of SM).

Aerosol volume size distribution

Figure 4a presents the averaged variation of aerosol volume size distribution (VSD) for different episodes between 2001 and 2014 over Beijing. The fine mode showed the maxima peak at radius of ~0.15 μm for all episodes. The coarse mode showed the maxima peak at radius of 2.2 μm on the dust days and 2.9 μm on the non-dust days and entire springtime (mean from 2001 to 2014). This value was significantly smaller than the measurements made in Yinchuan area throughout the year by Liu et al. (2008). Obviously, the VSDs were dominated by the coarse modes for different episodes, particularly on the dust days indicating the presence of mineral dust particles due to the dust storms. The different VSD peaks for dust and non-dust days are due to differences in other characteristics of the aerosol particles, as well as their radii. During the dust days, the coarse mode aerosol volume concentration in the atmosphere was about 5.0 times more than that during non-dust days, whereas no significant change was observed in the fine-mode aerosol VSD (Fig. 4a). A very similar variation in aerosol VSD during dust events has also been reported over Kanpur (Singh et al. 2004; Prasad and Singh 2007) and Lahore (Alam et al. 2014b). The volume concentration, effective radius, and volume median radius on the dust days were higher than those of non-dust days, implying the greater contribution of coarse particles to size spectra, when dust events occurred at Beijing.

Figure 4b illustrates the variations of aerosol VSD for different AODs at 440 nm during the dust and non-dust days. For fine mode, the magnitude of high AOD (~1.73) on non-dust days was larger than those of other episodes. The maximum peak of coarse mode on the dust days has observed at a radius 2.2 μm for all AODs, except for AOD equal to 0.23. However, the coarse mode showed a maximum peak at a radius between 2.9 and 3.8 μm for all AODs during non-dust episodes. From Fig. 4b, the volume concentrations showed an increased trend with AOD for all episodes. For example, the volume concentration of coarse mode on dust days reached 1.15 $\mu m^3\ \mu m^{-2}$ when AOD was 2.3, which is ~2.5 times higher than that with AOD equal to 0.6. The volume concentration of coarse mode showed a significant difference for different episodes, when AOD was same. Further, the volume concentrations of coarse mode having low AOD during dust events were higher than that of high AOD during non-dust episodes. For example, the

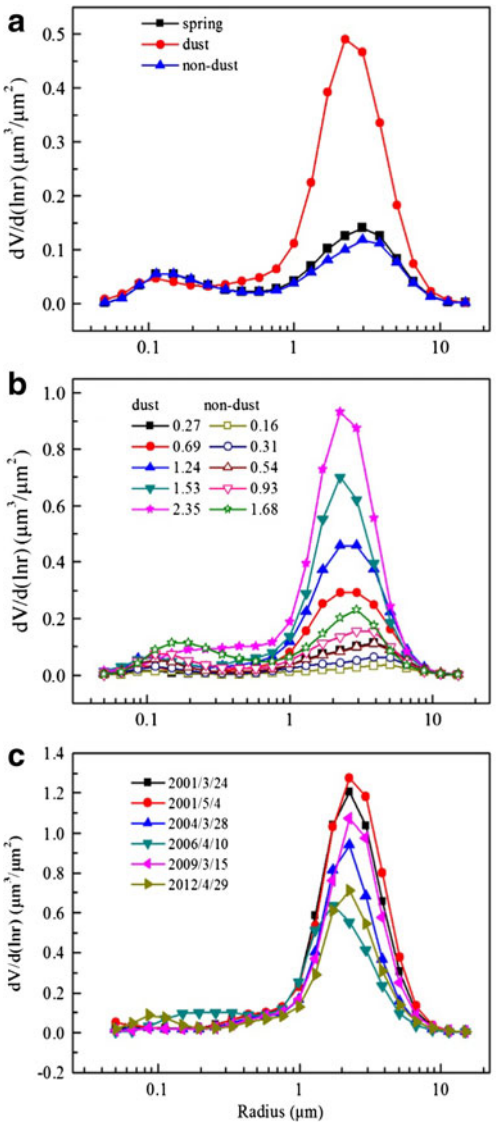

Fig. 4 Variations of aerosol volume size distributions during dust and non-dust days for the period 2001–2014 over Beijing: mean variations **a** for different episodes, **b** under different AOD conditions, and **c** on major dust days

volume concentration of coarse mode during non-dust episode was 0.30 $\mu m^3\ \mu m^{-2}$, when AOD was ~1.7. This is smaller than that of volume concentration of coarse mode when AOD was 0.6 and 3.0 times smaller when AOD was 1.47 during the dust episodes. This indicates that the local aerosol sources (such as wind derived soil dust, biomass burning, industrial pollution, and vehicular emissions) can be seen to have contributed to an increase in aerosol concentrations over urban Beijing in springtime (Xia et al. 2006; Wang et al. 2010). Further, it was observed that the aerosol VSD showed a mono-modal structure dominated with the coarse modes relative to fine mode on major dust days during 2001–2014 over Beijing (Fig. 4c). However, the VSDs were found to be a bi-modal pattern on 10 April 2006 and 29 April 2012, indicating the existence of fine particles. This result showed a good

agreement with the higher AE values noticed during the corresponding days (see Fig. 3a).

Spectral variations of single scattering albedo, asymmetry factor, and complex refractive index

The SSA showed a distinct variation with wavelength for different episodes. An increasing trend in SSA with spectral wavelengths has been observed during dust episodes, suggesting that the SSA is wavelength dependent. This increase in SSA with wavelength shows that aerosol particles are predominantly scattering in nature and larger in size, instead of absorbing particles (Singh et al. 2004). In contrast, during non-dust and spring days, an increasing trend at shorter wavelengths (440–670 nm) and a slow decreasing trend at the longer wavelengths (670–1020 nm) were observed (Fig. 5a). This was due to mixing with the anthropogenic aerosol pollution derived from the biomass burning and fossil fuel combustion (coal–petroleum) (Chameides et al. 1999). During dust days, the SSA fluctuated from 0.82 to 0.96 with an average value of 0.88 that occurred at a wavelength of 440 nm, which is lower than the SSA values obtained by Dubovik et al. (2002) for desert dust (0.92–0.93 at 440 nm). The maximum value (~0.96) of SSA during dust episode occurred at a wavelength of 1020 nm, which is an indication of the dust aerosol. This is higher and lower with the values (0.91 and 0.99) of SSA_{1020} reported by Alam et al. (2012, 2014b) over Lahore during summer season of 2011 and 2012, respectively.

Dubovik et al. (2002) found the spectral difference in ΔSSA ($SSA_{1020\ nm} - SSA_{440\ nm}$) to be greater than 0.05 for mineral dust particles. In our study, the spectral difference ΔSSA was 0.08 for dust days and matches well with the results made by Dubovik et al. (2002). The SSA varied between 0.74 and 0.99 with an average value of 0.89 at 440 nm in springtime during 2001–2014, which is similar to the results observed in spring of 2011–2012 over Shanghai (Cheng et al. 2015). The SSA at four wavelengths for different AODs on dust and non-dust days of spring during 2001–2014 is presented in Fig. 5b, in which the SSAs have been averaged and sorted according to the AOD measured at 440 nm. The SSA showed an increasing trend with AOD on dust days but varied with AOD in nonlinear approach on non-dust days. Mean SSA also showed a low sensitivity to AOD with an average value varying from 0.87 to 0.96 on dust days and 0.87 to 0.93 on non-dust days at the four wavelengths.

The variations in the total ASY over Beijing are shown in Fig. 5c–d. The ASY showed a lower sensitivity to longer wavelengths at 675–1020 nm when compared to the shorter wavelengths 440–675 nm (Fig. 5c). The average ASY value for the study period (2001–2014) in spring over urban Beijing at a wavelength of 440 nm was about 0.70, which is evidently higher than that of the other three wavelengths (an average of 0.65). When the dust storm attacked at Beijing, the averaged value of ASY was obviously enhanced at all four wavelengths. For example, the value of ASY on dust days reached to 0.73 at a wavelength 440 nm and 0.70 at the other three wavelengths. The higher value of ASY on dusty days at 440 nm reflects a dominance of dust particles in forward scattering over absorbing anthropogenic aerosols. Figure 5d shows the average of ASY at different AOD_{440} conditions on dust and non-dust days over Beijing. The ASY commonly showed a decreasing trend at the wavelengths of 440–870 nm and then slightly increases at the later wavelength for any AOD. But, the ASY showed a complete decreasing trend at all four wavelengths, when AOD reached the extreme high value.

The variations of real (Re) and imaginary (Im) parts of refractive index (RI) for different episodes and at different AODs are shown in Fig. 5e–h. The Re and Im parts of RI showed contrasting spectral behavior. In our study, Re part of RI shows a high value greater than 1.50 in all the four wavelengths in Beijing during dust days (Fig. 5e). This suggests that predominance of mineral dust transported aerosols from source to local region enhancing coarse particles, which are scattering rather than absorbing. The RI values for mineral dust particles have been reported by to be 1.53 ± 0.05 for Re and −0.006 or less for Im parts (Koepke et al. 1997). Our results are in close agreement with those investigated by Cheng et al. (2015) and Cao et al. (2014) over Shanghai and Beijing, respectively, during the dust days. The Im part of RI was found to be low (0.007) at all wavelengths during dust days compared with the non-dust and springtime events (Fig. 5g), indicating their non-absorbing nature. This also supported by the higher SSA which means higher scattering and lower absorption during dust days (see Fig. 5a). In addition, the RI–Im decreases with the increasing wavelength. This is similar with the findings observed by several researchers (e.g., Prasad and Singh 2007; Alam et al. 2012, 2014a, b; Cao et al. 2014). Overall variations in RI (both Re and Im components) within our study reveal that mineral dust particles are more dominant on dust days than other episodes.

Aerosol radiative forcing and efficiency

The daily averaged SW and LW ARF variations at the TOA and the BOA during the dust and non-dust days are shown in Fig. 6. The SW ARF values during dust days ranged between −166.66 and −236.02 W m^{-2} at the BOA and between −65.88 and −115.65 W m^{-2} at the TOA, given rise to an atmospheric forcing ranging between +86.72 and +133.67 W m^{-2} (Fig. 6a). The corresponding atmospheric HR varied from 2.44 to 3.76 K day^{-1} during major dust days for the study period over Beijing. Similarly, the SW ARF values have been presented for the non-dust events (see Fig. 6c). The LW ARF values during dust days ranged from +7.88 to +21.73 W m^{-2} at the BOA and from +6.33 to +25.88 W m^{-2} at the TOA. LW

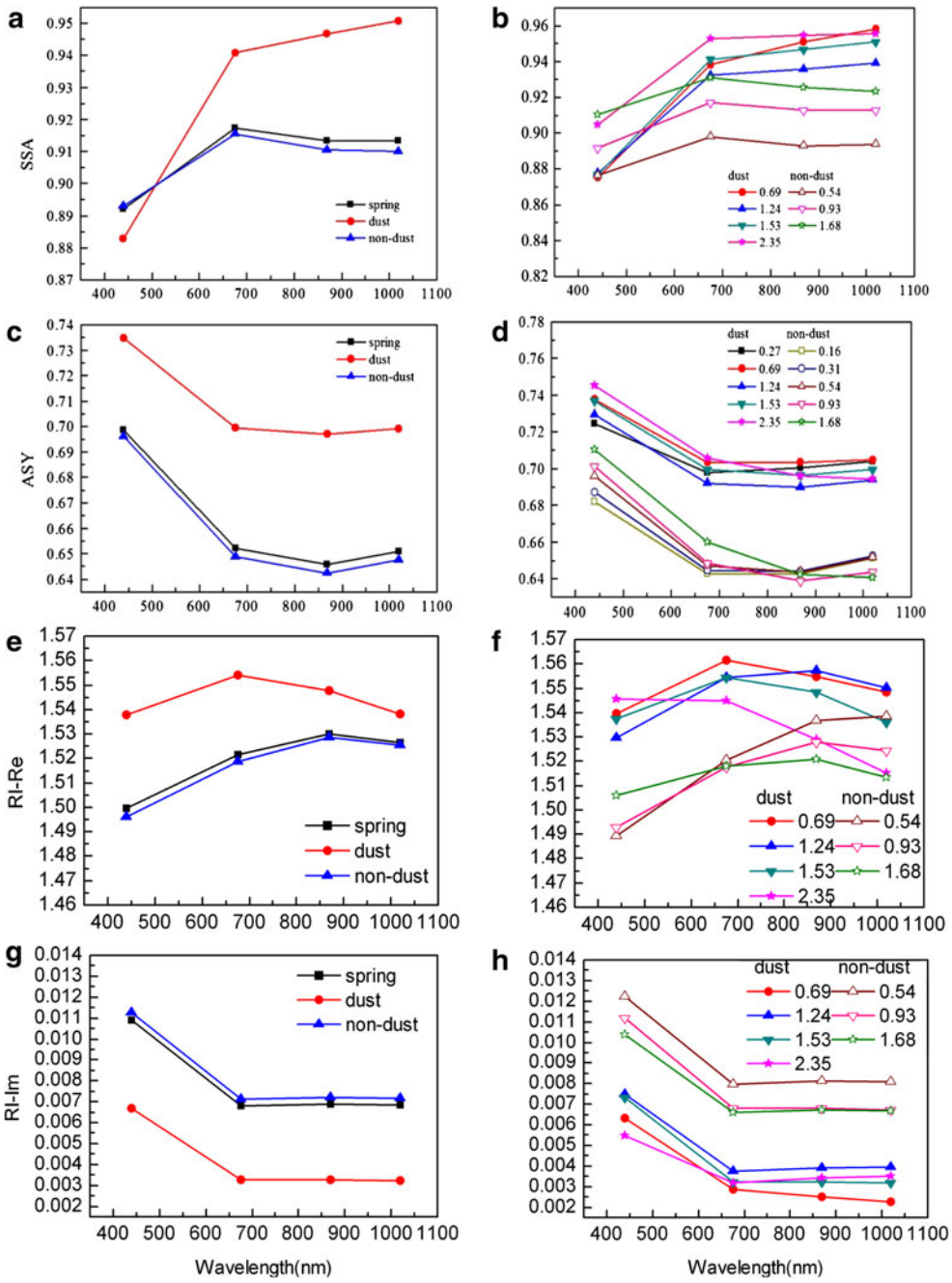

Fig. 5 Same as in Fig. 4 (except for the major dust days), but for **a**, **b** SSA, **c**, **d** ASY, **e**, **f** RI–Re, and **g**, **h** RI–Im

radiations are therefore shown to produce significant warming during dust days, both at the BOA and at the TOA.

The global mean SW ARF values at the BOA and the TOA have been found by several authors to be negative (e.g., Ge et al. 2010; Alam et al. 2012, 2014a, b; Srivastava et al. 2015; Yu et al. 2016 and references here in). Also, Alam et al. (2011) reported the averaged ARF at the TOA and the BOA of −22 ± 6 and −73 ± 12 W m^{-2}, respectively, over an urban city Karachi, Pakistan, for the 1-year period during August 2006–July 2007. It is also revealed from Table 2 that the comparison of TOA and BOA ARF retrieved from the AERONET and SBDART showed good agreement during dust and non-dust days. Overall, the BOA forcing is high for AERONET than SBDART and the TOA forcing is almost comparable for AERONET and SBDART. There is a large difference between the ARF values at the TOA and the BOA, indicating that solar radiation is being absorbed within the atmosphere, which results in the atmosphere becoming warmer but the earth's surface (BOA) becoming cooler (Alam et al. 2012, 2014b; Valenzuela et al. 2012; Yu et al. 2016 and references here in). The overall uncertainty in the estimated forcing due to deviations in model simulation has

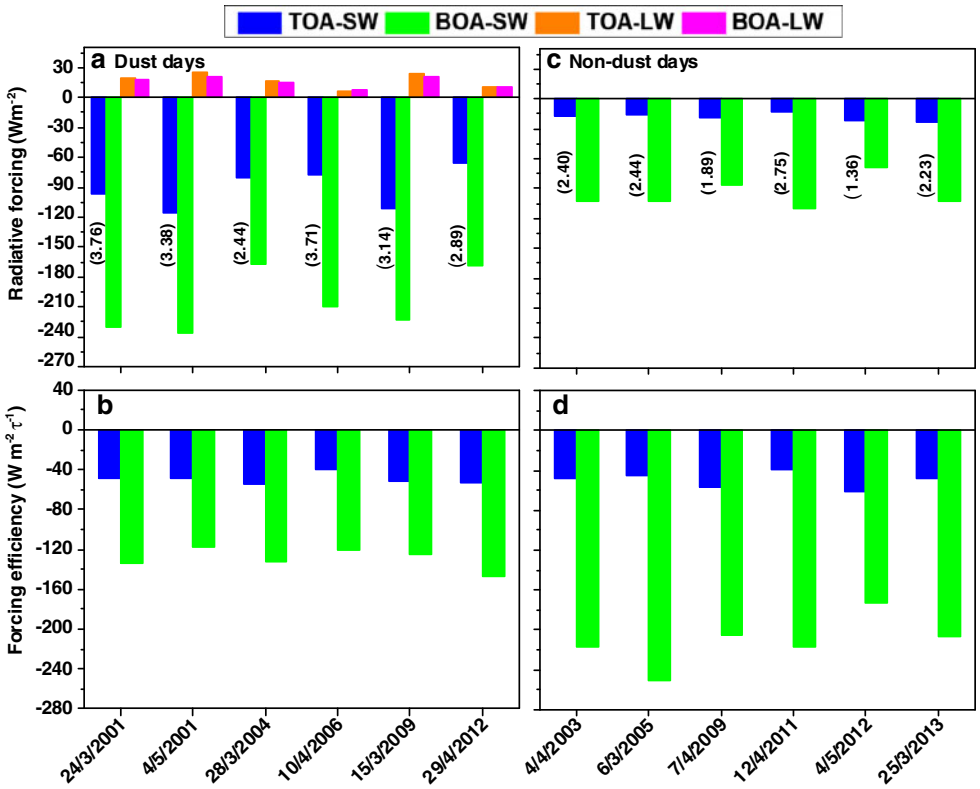

Fig. 6 **a** Shortwave and **c** longwave aerosol radiative forcing and **b**, **d** forcing efficiencies computed from SBDART model at the BOA and the TOA during major dust and non-dust days, respectively, over Beijing. The estimated heating rates for the corresponding ARF are shown *inside* **a**, **c** *within the parenthesis*

been previously reported by several authors (Alam et al. 2011, 2012, 2014a, b; Adesina et al. 2014; Valenzuela et al. 2012; Srivastava et al. 2015; Yu et al. 2016) and hence not repeated.

The aerosol radiative forcing efficiency (ARFE), calculated as daily ARF in the column atmosphere per unit of AOD (or τ) at 440 nm, was also investigated in this study. Thus, we have

Table 2 Comparison of AERONET-derived and SBDART-estimated shortwave ARF and ARFE at the TOA and the BOA during dust and non-dust days over Beijing

Date	AERONET				SBDART			
	ARF		ARFE		ARF		ARFE	
	TOA	BOA	TOA	BOA	TOA	BOA	TOA	BOA
Dust days								
2001 Mar 24	−103.93	−284.07	−49.01	−133.93	−97.11	−230.78	−45.18	−112.02
2001 May 04	−121.80	−293.83	−48.65	−117.35	−115.65	−236.02	−46.76	−96.11
2004 Mar 28	−88.04	−212.09	−54.87	−132.18	−79.94	−166.66	−50.40	−105.21
2006 Apr 10	−82.49	−249.41	−39.86	−120.51	−77.65	−209.69	−33.33	−114.32
2009 Mar 15	−115.25	−278.79	−51.53	−124.66	−111.78	−223.68	−50.29	−101.83
2012 Apr 29	−72.95	−203.20	−52.85	−147.23	−65.88	−168.84	−45.57	−126.95
Non-dust days								
2003 Apr 04	−27.65	−123.91	−48.47	−217.21	−17.75	−103.23	−23.70	−236.61
2005 Mar 06	−23.08	−129.08	−44.72	−250.15	−15.86	−102.54	−22.68	−265.56
2009 Apr 07	−28.61	−104.12	−56.48	−205.57	−19.16	−86.46	−29.34	−215.77
2011 Apr 12	−25.01	−137.96	−39.41	−217.43	−12.60	−110.43	−15.02	−222.65
2012 May 04	−28.20	−80.20	−60.57	−172.29	−21.07	−69.34	−36.78	−182.47
2013 Mar 25	−29.08	−127.14	−47.32	−206.85	−23.08	−102.38	−27.02	−229.84

ARF and ARFE are measured in terms of W m^{-2} and W m^{-2} τ^{-1}, respectively. Here, τ is AOD at 440 nm

computed ARFE, as the ratio of daily average ARF to the corresponding daily mean AOD_{440}, for both dust and non-dust days during the study period over Beijing. Figure 6b, d shows the ARFE values during the dust and non-dust days, respectively. The ARFE on dust days varied from −96.11 to −126.95 W $m^{-2}\tau^{-1}$ at the BOA and from −33.33 to −50.40 W $m^{-2}\tau^{-1}$ at the TOA (Fig. 6b). Similarly, the ARFE ranged between −182.47 W $m^{-2}\tau^{-1}$ (−15.02 W $m^{-2}\tau^{-1}$) and −265.56 W $m^{-2}\tau^{-1}$ (−27.02 W $m^{-2}\tau^{-1}$) at the BOA (TOA) during non-dust days (Fig. 6d).

Conclusions

The long-term characteristics of aerosol optical, microphysical, and radiative properties during major dust storm events in spring were presented from the AERONET's Sunphotometer measurements over urban Beijing between 2001 and 2014. The seasonal averaged AOD during springtime was about 0.78 at the wavelength of 440 nm. During dust days, the averaged AOD_{440} increased to 1.20 and $AE_{440–870}$ decreased to 0.44, which indicated a high aerosol loading over the region and serious impact on human health. In addition to aerosols, API showed higher values during dust days due to poor air quality. The maximum aerosol VSDs occurred during dust events with a higher volume concentration, effective radius, and volume median radius. The volume concentrations showed an increased trend with AOD for all episodes during the period of study. The SSA on dust days was much higher (more scattering type relative to absorbing) than that in other episodes, with an average value of 0.88 at 440 nm. When the dust attacked in Beijing, the averaged value of ASY was obviously enhanced at any wavelengths, attributed to the higher contribution of large particles. The real (imaginary) part of RI showed higher (lower) values in all the four wavelengths during dust days, indicating dominance of scattering aerosols over Beijing. The SBDART model simulation revealed that SW (LW) ARF produces cooling (warming) effects both at the TOA and at the BOA on dust days.

Acknowledgments The present work was mainly supported by the "Strategic Priority Research Program (B)" of the Chinese Academy of Sciences (Grant No. XDB05030104), the National Natural Science Foundation of China (Grant Nos. 41475142, 41575133), the Key Laboratory for Aerosol-Cloud-Precipitation of the China Meteorological Administration, NUIST (Grant Nos. KDW1102, KDW1404), the Qing Lan Project, and the Priority Academic Program Development (PAPD) of Jiangsu Higher Education Institutions. Concerning to the AERONET data used in this paper, we are particularly grateful to the PIs, Prof. Hongbin Chen, and Prof. Philippe Goloub for their efforts in establishing and maintaining the Beijing site and their assistants for the upkeep of the instrument and availability of the online data. We also thank the MODIS and CALIPSO scientific teams and also the NOAA Air Resources Laboratory (ARL) for the provision of the HYSPLIT transport and dispersion model used in this study. The authors would like to acknowledge Prof. Gerhard Lammel, the Editor-in-Chief of the journal, and the anonymous reviewers for their helpful comments and constructive suggestions toward the improvement of an earlier version of the manuscript.

References

Adesina AJ, Kumar KR, Sivakumar V, Griffith D (2014) Direct radiative forcing of urban aerosols over Pretoria (25.75°S, 28.28°E) using AERONET Sunphotometer data: first scientific results and environmental impact. J Environ Sci 26:2459–2474

Alam K, Trautmann T, Blaschke T (2011) Aerosol optical properties and radiative forcing over mega-city Karachi. Atmos Res 101:773–782

Alam K, Trautmann T, Blaschke T, Majid H (2012) Aerosol optical and radiative properties during summer and winter season over Lahore and Karachi. Atmos Environ 50:234–245

Alam K, Sahar N, Iqbal Y (2014a) Aerosol characteristics and radiative forcing during pre-monsoon and post-monsoon seasons in an urban environment. Aerosol Air Qual Res 14(1):99–107

Alam K, Trautmann T, Blaschke T, Subhan F (2014b) Changes in aerosol optical properties due to dust storms in the Middle East and Southwest Asia. Remote Sens Environ 143:216–227

Alpert P, Kaufman YJ, Shay-El Y, Tanre D, da Silva A, Schubert S et al (1998) Quantification of dust-forced heating of the lower troposphere. Nature 395:367–370

Cao C, Zheng S, Singh RP (2014) Characteristics of aerosol optical properties and meteorological parameters during three major dust events (2005–2010) over Beijing, China. Atmos Res 150:129–142

Chameides WL, Yu H, Liu SC, Bergin M, Zhou X, Mearns L et al (1999) Case study of the effects of atmospheric aerosols and regional haze on agriculture: an opportunity to enhance crop yields in China through emission controls. Proc Natl Acad Sci 96:13626–13633

Cheng T, Xu C, Duan J, Wang Y, Leng C, Tao J, Che H, He Q, Wu Y, Zhang R, Li X, Chen J, Kong L, Yu X (2015) Seasonal variation and difference of aerosol optical properties in columnar and surface atmospheres over Shanghai. Atmos Environ. doi:10.1016./j.atmosenv.2015.05.029

Draxler RR, Rolph GD (2013) HYSPLIT (HYbrid Single-Particle Lagrangian Integrated Trajectory) Model access via NOAA ARL READY (Website (http://www.arl.noaa.gov/HYSPLIT.php)) NOAA Air Resources Laboratory, College Park, MD

Dubovik OA, Smirnov A, Holben BN, King MD, Kaufman YJ, Eck TF, Slutsker I (2000) Accuracy assessments of aerosol properties retrieved from Aerosol Robotic Network (AERONET) sun and sky measurements. J Geophys Res 105:9791–9806

Dubovik O, Holben BN, Eck TF, Smirnov A, Kaufman YJ, King MD, Tanré D, Slutsker I (2002) Variability of absorption and optical properties of key aerosol types observed in worldwide locations. J Atmos Sci 59:590–608

Eck TF, Holben BN, Dubovik O, Smirnov A, Goloub P, Chen HB, Chatenet B, Gomes L, Zhang XY, Tsay S-C (2005) Columnar aerosol optical properties at AERONET sites in central eastern Asia and aerosol transport to the tropical mid-Pacific. J Geophys Res 110(D6):1984–2012

Ge JM, Su J, Ackerman TP, Fu Q, Huang JP, Shi JS (2010) Dust aerosol optical properties retrieval and radiative forcing over northwestern China during the 2008 China–U.S. joint field experiment. J Geophys Res 115(D00k12). Doi: 10.1029/2009JD013263

Holben BN, Eck TF, Slutsker I, Tanré D, Buis JP, Setzer A, Vermote E, Reagan JA, Kaufman Y, Nakajima T, Lavenu F, Jankowiak I, Smirnov A (1998) AERONET-A federated instrument network

and data archive for aerosol characterization. Remote Sens Environ 66:1–16

IPCC (2013) Climate change 2013: the physical science basis: contribution of Working Group I to the Fifth Assessment Report of the Intergovernmental Panel on Climate Change (IPCC). In: Stocker TF, Qin D, Plattner GK, Tignor M, Allen SK, Boschung J, Nauels A, Xia Y, Bex V, Midgley PM (Eds). Cambridge University Press, Cambridge, p 1535

Koepke P, Hess M, Schult I, Shettle EP (1997) Global aerosol data set Rep., 243. Hamburg, Germany: Max Planck Inst for Meteorol 44

Lau KM, Kim MK, Kim KM (2006) Asian summer monsoon anomalies induced by aerosol direct forcing: the role of the Tibetan Plateau. Climate Dynam 26:855–864. doi:10.1007/s00382-006-0114-z

Lee J, Kim J, Song CH, Kim SB, Chun Y, Sohn BJ, Holben BN (2010) Characteristics of aerosol types from AERONET sunphotometer measurements. Atmos Environ 44:3110–3117

Li LJ, Wang Y, Li JX, Xin LZ, Jin J (2012) The analysis of heavy air pollution in Beijing during 2000~2010. China Environ Sci 32(1): 23–30 (Chinese)

Liao H, Seinfeld JH (1998) Radiative forcing by mineral dust aerosols: sensitivity to key variables. J Geophys Res 103(D24):31637–31645

Liou KN (2002) An introduction to atmospheric radiation. Elsevier, New York, p 583

Liu J, Zheng Y, Li Z, Wu R (2008) Ground-based remote sensing of aerosol optical properties in one city in Northwest China. Atmos Res 89:194–205

Miller RL, Tegen I, Perlwitz J (2004) Surface radiative forcing by soil dust aerosols and the hydrologic cycle. J Geophys Res 109, D04203. doi:10.1029/2003JD004085

Prasad AK, Singh RP (2007) Changes in aerosol parameters during major dust storm events (2001–2005) over the Indo-Gangetic Plains using AERONET and MODIS data. J Geophys Res 112(D9):1984–2012

Ramanathan V, Crutzen PJ, Kiehl JT, Rosenfeld D (2001) Aerosols, climate, and the hydrological cycle. Science 294:2119–2124

Ricchiazzi P, Yang S, Gautier C, Sowle D (1998) SBDART: a research and teaching software tool for plane-parallel radiative transfer in the earth's atmosphere. Bull Am Meteorol Soc 79:2101–2114

Shen XX, Liu CS, Shi RH, Bai KX, Wang C, Gao W (2013) Preliminary study of a dust event over Beijing by using satellite data and ground-based measurements. Proc SPIE 8869, Remote Sensing and Modeling of Ecosystems for Sustainability X 886912:886911–886912

Singh RP, Dey S, Tripathi S, Tare V, Holben BN (2004) Variability of aerosol parameters over Kanpur, northern India. J Geophys Res 109(D23206). doi: 10.1029/2004JD004966

Smirnov A, Holben BN, Eck TF, Dubovik O, Slutsker I (2000) Cloud screening and quality control algorithms for the AERONET database. Remote Sens Environ 73:337–349

Smirnov A, Holben BN, Kaufman YJ, Dubovik O, Eck TF, Slutsker I, Pietras C, Halthore RN (2002) Optical properties of atmospheric aerosol in maritime environments. J Atmos Sci 59:501–523

Srivastava AK, Ram K, Singh S, Kumar S, Tiwari S (2015) Aerosol optical properties and radiative effects over Manora Peak in the Himalayan foothills: seasonal variability and role of transported aerosols. Sci Total Environ 502:287–295

Tegen I, Werner M, Harrison S, Kohfeld K (2004) Relative importance of climate and land use in determining present and future global soil dust emission. Geophys Res Lett 31, L05105

Valenzuela A, Olmo EJ, Lyamani H, Anton M, Quirantes A, Alados-Arboledas L (2012) Aerosol radiative forcing during African desert dust events (2005–2010) over Southeastern Spain. Atmos Chem Phys 12:10331–10351

Valenzuela A, Olmo FJ, Lyamani H, Antón M, Titos G, Cazorla A, Alados-Arboledas L (2015) Aerosol scattering and absorption Angström exponents as indicators of dust and dust-free days over Granada (Spain). Atmos Res 154:1–13

Wang WJ, Cheng TT, Zhang RJ, Jia X, Han ZW, Zhang XL, Xu XF, Li DP (2010) Insights into an Asian dust event sweeping Beijing during April 2006: particle chemical composition, boundary layer structure, and radiative forcing. J Geophys Res 115, D18208. doi:10.1029/2009JD013391

Wang YJ, Xin Z, Li WS, Wang P, Hao WM, Nordgren BL, Chen H, Wang L, Sun Y (2011) Seasonal variations in aerosol optical properties over China. J Geophys Res 116, D18209. doi:10.1029/2010JD015376

Winker DM, Pelon J, McCormick MP (2003) The CALIPSO mission: Spaceborne lidar for observation of aerosols and clouds. Proc SPIE 4893:1–11

Wu Y, Zhu J, Che H, Xia X, Zhang R (2015) Column-integrated aerosol optical properties and direct radiative forcing based on sun photometer measurements at a semi-arid rural site in Northeast China. Atmos Res 157:56–65

Xia XA, Chen HB, Wang PC (2004) Aerosol properties in a Chinese semiarid region. Atmos Environ 38(27):4571–4581

Xia XA, Chen HB, Wang PC, Zhang WX, Goloub P, Chatenet B, Eck TF, Holben BN (2006) Variation of column-integrated aerosol properties in a Chinese urban region. J Geophys Res 111, D05204. doi:10.1029/2005JD006203

Xu WS, Wei Q, Feng P, Zhao Y, Hu LL (2012) The effects of dust weather on air quality and its synoptic type in spring 2010 of Beijing. Environ Monit 28(6):19–27 (Chinese)

Xu C, Ma YM, You C, Zhu ZK (2015) The regional distribution characteristics of aerosol optical depth over the Tibetan Plateau. Atmos Chem Phys Discuss 15:15683–15710. doi:10.5194/acpd-15-15683-2015

Yan N, Wu G, Zhang X, Zhang C, Xu T, Zhu L (2015) Variation of aerosol optical properties from AERONET observation at Mt. Muztagh Ata, Eastern Pamirs. Atmos Res 153:480–488

Yu XN, Zhu B, Zhang MG (2009) Seasonal variability of aerosol optical properties over Beijing. Atmos Environ 43(26):4095–4101

Yu XN, Zhu B, Yin Y, Yang J, Li YW, Bu XL (2011) A comparative analysis of aerosol properties in dust and haze-fog days in a Chinese urban region. Atmos Res 99:241–247

Yu XN, Zhang HJ, Deng Z, De Q, Kang N (2012) Aerosol optical properties during dusty events in source and downwind regions. J Desert Res 32(6):1710–1715 (Chinese)

Yu XN, Shi CZ, Ma J, Zhu B, Li M, Wang J, Yang SY, Kang N (2013) Aerosol optical properties during firework, biomass burning and dust episodes in Beijing. Atmos Environ 81:475–484

Yu XN, Kumar KR, Lu R, Ma J (2016) Changes in column aerosol optical properties during extreme haze-fog episodes in January 2013 over urban Beijing. Environ Pollut 210:217–226

Zheng S, Cao CX, Singh RP (2014) Comparison of ground based indices (API and AQI) with satellite based aerosol products. Sci Total Environ 488:398–412

Zhuang G, Guo J, Yuan H, Zhao C (2001) The compositions, sources and size distribution of the dust storm from China in spring of 2000 and its impact on the global environment. Chin Sci Bull 46:895–901